All polymer asymmetric Mach–Zehnder interferometer waveguide sensor by imprinting bonding and laser polishing*

Yu Liu(刘豫), Yue Sun(孙月), Yun-Ji Yi(衣云骥)†, Liang Tian(田亮), Yue Cao(曹悦), Chang-Ming Chen(陈长鸣), Xiao-Qiang Sun(孙小强), and Da-Ming Zhang(张大明)

State Key Laboratory on Integrated Optoelectronics, College of Electronic Science and Engineering, Jilin University, Changchun 130012, *China*

(Received 29 June 2017; revised manuscript received 30 August 2017; published online 20 November 2017)

We present an all polymer asymmetric Mach–Zehnder interferometer (AMZI) waveguide sensor based on imprinting bonding and laser polishing method. The fabrication methods are compatible with high accuracy waveguide sensing structure. The rectangle waveguide structure of this sensor has three sensing surfaces contacting the test media, and its sensing accuracy can be increased 5 times compared with that of one surface sensing structure. An AMZI device structure is designed. The single mode condition, the length of the sensing arm, and the length deviation between the sensing arm and the reference arm are optimized. The length deviation is optimized to be 19.8 μm in a refractive index range between 1.470 and 1.545. We fabricate the AMZI waveguide by lithography and wet etching method. The imprinting bonding and laser polishing method is proposed and investigated. The insertion loss is between −80.36 dB and −10.63 dB. The average and linear sensitivity are 768.1 dB/RIU and 548.95 dB/RIU, respectively. And the average and linear detection resolution of the sensor are 1.30×10^{-6} RIU (RIU: refractive index unit) and 1.82×10^{-5} RIU, respectively. This sensor has a fast and cost-effective fabrication process which can be used in the cases of requiring portability and disposability.

Keywords: integrated optics devices, polymer waveguides, sensors, microstructure fabrication

PACS: 42.79.Gn, 42.70.Jk, 42.81.Pa, 42.79.–e **DOI:** 10.1088/1674-1056/26/12/124215

1. Introduction

Optical waveguide devices are commonly utilized in modern sensing technology. They possess anti-electromagnetic interference, simple structure, sensor miniaturization, and multi-channel synchronous detection, making them well-suited to multiple application environments such as seismic exploration, environmental pollution, and medical diagnostics. Optical waveguide sensors can be divided by their material into inorganic waveguide sensor and polymer waveguide sensor categories. The inorganic waveguide sensors are highly sensitive due to their inherently high refractive index deviations, while polymer waveguide sensors have the advantages of low cost, and easy modification as necessary; they are also very useful in sensing applications that require portability and disposability.[1]

Polymer optical waveguide sensors have several main structures such as surface plasma resonance (SPR) structures,[2–6] grating structures,[7,8] micro-ring structures, and MZI structures. The SPR structure comprises a commercial chemical detection system based on prism-coupling technology. It is disadvantaged by its sensitivity to temperature and test medium composition; its gold film also causes optical loss. The grating period of the grating structure is very short: on the order of only several hundred nanometers, but it comes with stringent fabrication process and spectral analysis requirements. Longer grating periods are sensitive to temperature and external stress.[9–11] The radius of the micro-ring structure is several tens of micrometers, i.e., it is attractive in the sense of sensor miniaturization. The optical signal resonance phenomenon increases the equivalent contact length of the waveguide and test medium significantly to ensure sufficient sensitivity. It is challenging that high-precision fabrication process is necessary to control the coupling distance between the micro-ring and straight waveguide, however.[12] Further, the micro-ring can lead to additional bending loss. One branch waveguide serves as a sensing arm in the MZI structure while a second branch is used as a reference arm. By removing the upper cladding layer of the waveguide from the sensing arm, the evanescent field of the light wave in the core layer can be forced to contact the test medium.[13] The test medium has a fluctuating refractive index which influences the phase of optical fields between sensing and reference arms. The phase shift causes the output optical power to fluctuate as well. The MZI structure is cost-effective and easily fabricated; it does not require spectral detection and can realize simultaneous multi-channel detection.[14]

The MZI structure requires that the sensing window be etched, followed by a careful process to align the waveguide with lithography mask of the microfluidic layer. The AMZI structure, a subclass of MZI structures, does not require the alignment or etching processes. The microfluidic channel

*Project supported by the National Natural Science Foundation of China (Grant Nos. 61605057, 61475061, and 61575076), the Science and Technology Development Plan of Jilin Province, China (Grant No. 20140519006JH), and the Excellent Youth Foundation of Jilin Province, China (Grant No. 20170520158JH).

†Corresponding author. E-mail: yiyj@jlu.edu.cn

© 2017 Chinese Physical Society and IOP Publishing Ltd

is integrated onto the waveguide in the AMZI sensor. Because the sensitivity is proportional to the length deviation of waveguide branch, the length deviation can be introduced in *Y* branches or MZI arms. Compared with the MZI sensor, the AMZI sensor has low sensitivity, due to the length deviation of *Y* branches. And longer length deviation means greater sensitivity.

In the last decade, MZI waveguide sensor has made much progress. In 2008, the MZI waveguide chemical sensor with inverted ridge structure was presented by Shew *et al*.[15] They detected the antigen concentration by combining covalent bond with antibody as the sensitive layer of the waveguide. The sensitivity of the sensor was 10^{-12}g/ml. In 2011, Bruck *et al*. produced an inverted ridge MZI waveguide sensor on the SiO_2 substrate, and the detection accuracy of streptavidin could reached 0.1 μg/ml.[16] In 2012, Wang *et al*. presented an improved sensing window with three sensing surfaces, whose sensitivity could be enhanced by a factor of 2.8 in theory.[17] In 2014, Ozhikandathil and Packirisamy[18] made a multiple *Y*-branch MZI waveguide sensor with microfluidic layer. This sensor was used for detecting the fluorophore tagged recombinant bovine somatotropin, and the detection limit of fluorophore tagged recombinant bovine somatotropin was 120 ng/ml. In the inorganic waveguide sensing area, different kinds of waveguide structures were widely used in the sensing area. In the polymer waveguide sensing area, the three-sensing surface waveguide was rarely reported, because the integration of polymer waveguides and microfluidic channels are usually integrated by spin-coating and plasma treatment method. Spin coating would cover the waveguide, and the plasma etching method would add additional process and increase the surface roughness of the waveguide which would reduce the waveguide sensor properties.[14] In addition, the end face treatment of the integration device of the waveguide and the microfluidic channels is another problem. Because the thickness values of the waveguide and microfluidic channel integrated devices are usually larger than the blade depth of the dicing saw. And the polishing parameters of waveguide material and microfluidic channel material are usually incompatible with each other.

In this study, an integration method of polymer rectangle waveguide and polymer microfluidic channels is proposed to create an all-polymer, rectangular AMZI waveguide with three smooth surfaces. Instead of plasma treatment bonding and dicing saw cutting, the imprinting method and laser cutting method are introduced. The device has a higher sensitivity than the polymer inverted ridge structure or polymer rectangular waveguide structure with a single sensing surface, and it can be fabricated quickly from low-cost material (poly-methyl-methacrylate, PMMA), making it a promising approach to new devices that are highly portable and disposable.

2. Design and optimization

2.1. Material selection and single mode condition

SU-8 (Microchem Co., USA) polymer photoresist material and the PMMA (poly-methyl-methacrylate) are selected as the waveguide material due to the processability and smooth surface of SU-8 and the low cost and adjustable refractive index of PMMA.[19,20]

The sensitivities of waveguides with different materials matched are discussed. When PMMA is used as the substrate and cladding material, SU-8 or high index PMMA can be selected as the core material. The effective refractive index of the waveguide is calculated using the effective refractive index method to compare the sensitivities of these two core materials. The wavelength of the optical field is 1550 nm. As shown in Fig. 1, curves A (TE0 mode) and B (TM0 mode) are the ratio of $\partial N_{\text{eff}}/\partial n_{\text{c}}$ (N_{eff} is the effective refractive index, n_{c} is the refractive index of the test medium) when SU-8 (refractive index n=1.571) serves as the core layer and PMMA ($n = 1.495$) is used as the substrate layer. The size of the core is 2 μm×2 μm. C (TE0 mode) and D (TM0 mode) are the ratio of $\partial N\text{eff}/\partial n_{\text{c}}$ when PMMA (n=1.495) is used as the core layer and PMMA ($n = 1.483$) serves as the substrate layer. The size of the core is 2 μm×2 μm. Under single-mode condition, E (TE0 mode) and F (TM0 mode) are the ratio of $\partial Neff/\partial nc$ when PMMA (n=1.495) serves as the core layer and PMMA ($n = 1.483$) is used as the substrate layer. The size of the core is 5 μm×5 μm. The sensitivity increases as $\partial N_{\text{eff}}/\partial n_{\text{c}}$ increases. Large variation in refractive index between the core and the cladding enables higher sensing accuracy, so a waveguide with SU-8 as the core facilitates higher sensitivity than the waveguide with PMMA as the core.

The SU-8 2002 ($n = 1.571$) serves as the core material in the AMZI sensor. The PMMA ($n = 1.495$) is used as the substrate and micro reservoir material. The effective index method is used to investigate the single-mode transmission conditions of the SU-8 rectangular waveguide with an optical field wavelength of 1550 nm. As shown in Eq. (1), k_0 is the vacuum wave number, N_1 is the effective refractive index of the rectangular waveguide, n_1–n_4 are the refractive indice of four regions in Marcatili's method, and b is the thickness of core layer. As shown in Fig. 2, E^y_{mn} is the electric field of E_{mn} mode along the Y direction. Single-mode transmission can be achieved when the core layer height and width are both 2 μm.

$$\begin{aligned} & k_0(n_1^2 - N_1^2)^{1/2} b \\ = \; & n\pi + \arctan \frac{(N_1^2 - n_2^2)^{1/2}}{(n_1^2 - N_1^2)^{1/2}} \\ & + \arctan \frac{(N_1^2 - n_4^2)^{1/2}}{(n_1^2 - N_1^2)^{1/2}}, \quad (n = 0, 1, 2, \ldots) \end{aligned} \tag{1}$$

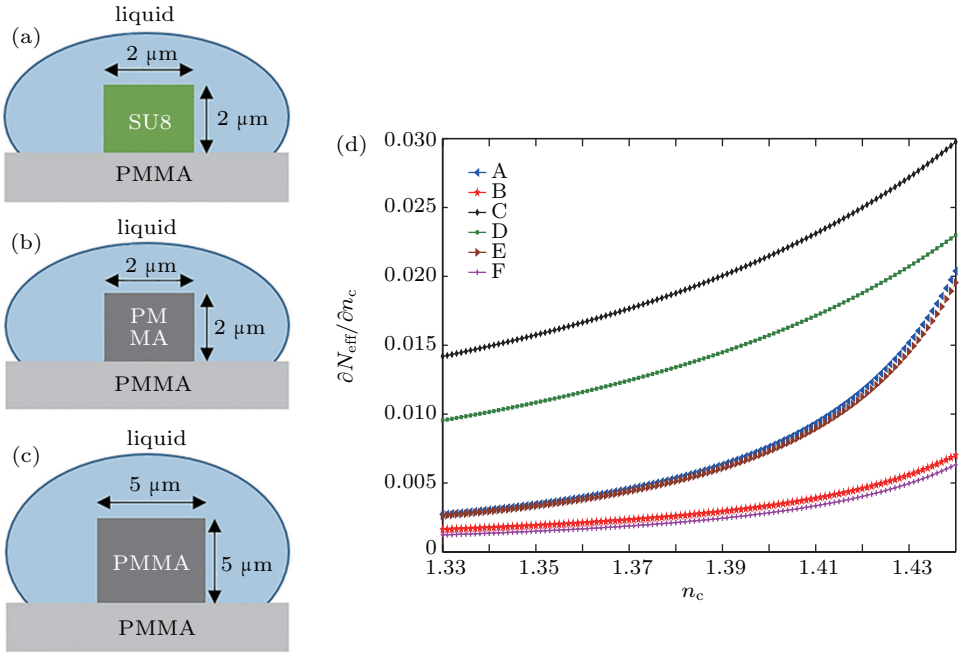


Fig. 1. (color online) Schematics of cross section of waveguide (a) when SU-8 ($n = 1.571$) serves as the core layer and PMMA ($n = 1.495$) is used as the substrate layer, (b) when PMMA ($n = 1.495$) serves as the core layer and PMMA ($n = 1.483$) is used as the substrate layer, (c) when PMMA ($n = 1.495$) serves as the core layer and PMMA ($n = 1.483$) is used as the substrate layer; (d) variations of $\partial N_{\rm eff}/\partial n_{\rm c}$ with $n_{\rm c}$.

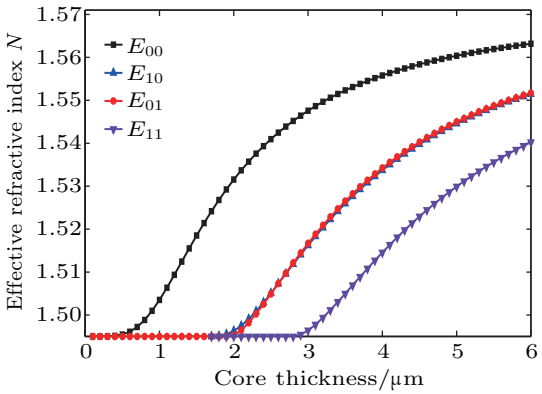


Fig. 2. (color online) Plots of effective refractive index versus SU-8 core layer thickness.

2.2. Waveguide contact method

In the AMZI sensor, it is assumed that ϕ_0 is the input optical field amplitude and ω_0 is the optical field angular frequency, and ζ_i is the phase shift introduced by the 3-dB beam splitter. The optical field is divided into two beams through the Y branches, which are expressed as follows:

$$\varphi_i(t) = \frac{\varphi_0}{\sqrt{2}} \exp(\mathrm{j}\omega_0 t - \zeta_i), \quad (i = 1, 2), \tag{2}$$

where θ_1 and θ_2 represent the phase shifts, which are introduced by the sensing arm and reference arm, respectively. The output optical field intensity is

$$I_{\rm out} = |\varphi(t)|^2 = |\varphi_0|^2 \cos^2 \left\{ \frac{1}{2}[2(\zeta_2 - \zeta_1) + (\theta_2 - \theta_1)] \right\}. \tag{3}$$

In an ideal situation,

$$I_{\rm out} = |\varphi_0|^2 \frac{1 + \cos(\theta_2 - \theta_1)}{2} = |\varphi_0|^2 \frac{1 + \cos(\Delta\theta)}{2}, \tag{4}$$

$$\Delta\theta = \theta_2 - \theta_1 = \frac{2\pi}{\lambda} \times \Delta L \times N_{\rm eff}. \tag{5}$$

where $N_{\rm eff}$ is the effective refractive index, ΔL is the length deviation of two branches, and λ is the light wavelength ($\lambda = 1550$ nm).

The sensitivity of the waveguide sensor can be expressed as

$$S = \frac{\partial I_{\rm out}}{\partial n_{\rm c}} = \frac{|\varphi_0|^2 \pi \Delta L}{\lambda} \cdot \sin\left(\frac{2\pi \Delta L}{\lambda} N_{\rm eff}\right) \cdot \frac{\partial N_{\rm eff}}{\partial n_{\rm c}}, \tag{6}$$

where S is the sensitivity of the sensor and $n_{\rm c}$ is the refractive index of the test medium.

Assume that $N_{\rm eff1}$, $N_{\rm eff2}$, and $N_{\rm eff3}$ are the effective refractive indices of the rectangular waveguide structure with one sensing surface contacting the test medium, the rectangular waveguide structure with three sensing surfaces contacting the test medium, and the inverted ridge waveguide structure respectively. The curves of $N_{\rm eff1}$, $N_{\rm eff2}$, and $N_{\rm eff3}$ are obtained as shown in Fig. 3. The proposed three-surface structure has a considerably higher sensing sensitivity which is 5.5 and 5.24 times those of the other two structures, respectively.

2.3. Asymmetric Mach–Zehnder interferometer (AMZI) design

According to the waveguide we designed, an AMZI structure is optimized due to its alignment-free property. Length deviation is introduced in the straight waveguide branch of the AMZI to improve its sensitivity. Compared with the length deviation of an AMZI structure in which the length deviation is introduced in Y branches, the length deviation introduced

in the straight waveguide branch is unlimited. It is necessary, however, to ensure that for the length deviation introduced in the straight waveguide branch, the output optical power varies monotonically in the sensing range. Excessive length deviation will increase the size of the device and its transmission loss.

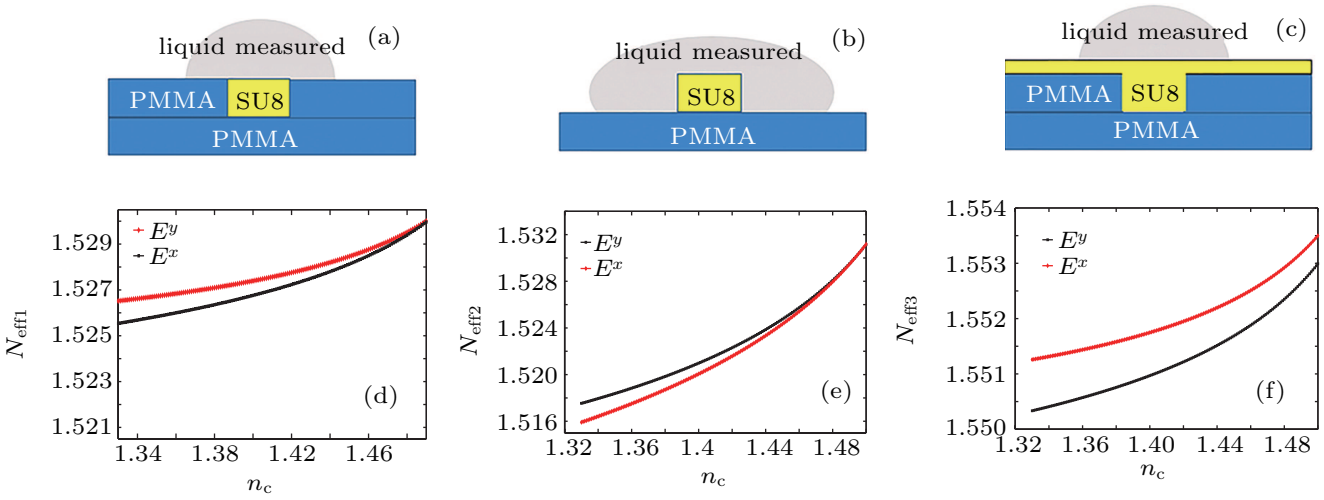


Fig. 3. (color online) Relationshis between N_{eff} and n_c for (a) rectangular waveguide structure with one surface contacting the test medium, (b) optimization rectangular waveguide structure with three surfaces contacting the test medium, (c) inverted ridge waveguide structure. (d) Schematic diagram of cross section of rectangular waveguide structure with one surface contacting the test media. (e) Schematic diagram of cross section of rectangular waveguide structure which has three surfaces contacting the test medium. (f) Schematic diagram of cross section of inverted ridge waveguide structure.

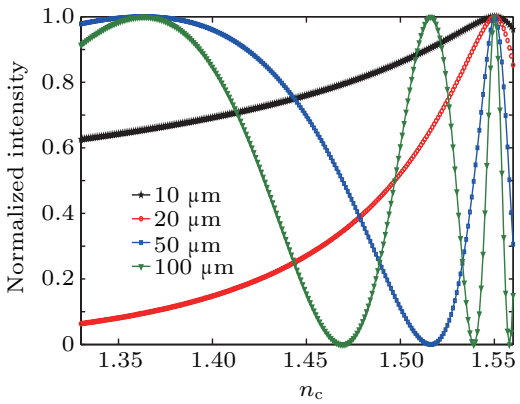


Fig. 4. (color online) Relationships between normalized output optical intensity and refractive index of n_c at different values of length deviation L.

The curves of normalized output optical intensity with different values of length deviation L are shown in Fig. 4. The largest slope of the curve is situated at the effective refractive index. In a fixed sensing range, the L is determined by the monotonicity and variation of output power. Output power variations determine the optimal value of L. As shown in Fig. 4, the curve slopes are largest at the values of n_e in a range of 1.470–1.545.

We also explore an optical power measurement system with the output optical power varying in a range of −70 dB–0 dB. In a range of 10 μm–20 μm, the variation of output optical power reaches its maximum value, when $L = 19.8$ μm in the range of 1.470–1.545. As shown in Fig. 5, the curve of normalized output optical intensity increases monotonically in the range of 1.470–1.545. The structure can be designed in the same manner in other sensing ranges.

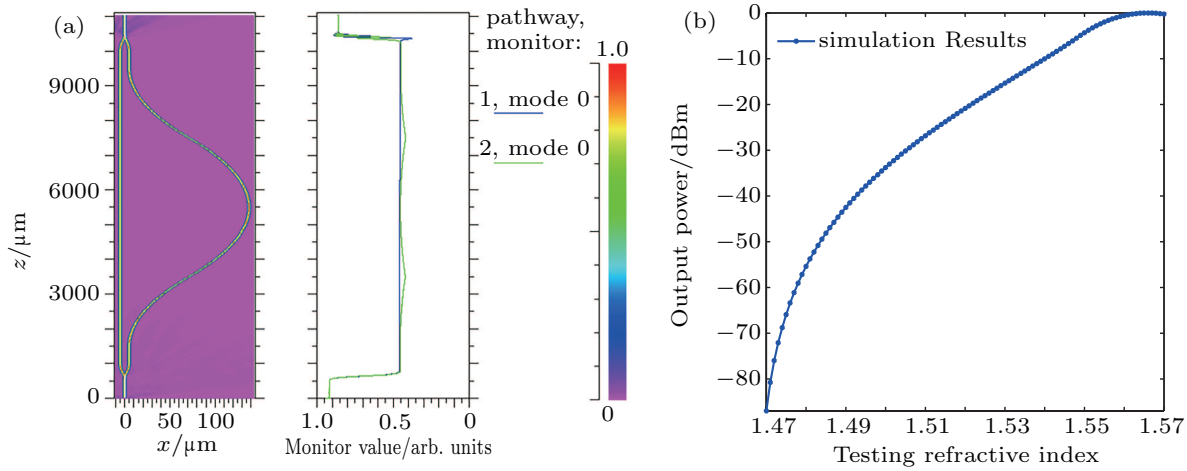


Fig. 5. (color online) (a) Simulated optical field when ΔL is 19.8 μm. (b) Normalized output optical intensity curve of sensor when ΔL is 19.8 μm.

The relationship between output optical power and normalized output optical intensity is

$$\text{Output} = 10 \times \log(I_{\text{out}}/I_{\text{in}}). \tag{7}$$

Because the low bending loss of cosine curve,[21] the cosine and straight type of lines are introduced in the two arms of the MZ structure. The cosine function is

$$y = a\cos\left(\frac{\pi x}{b}\right). \tag{8}$$

where a and b are the parameters, x is the direction of light propagation in the waveguide, and y is perpendicular to x. When length deviation L is 19.8 μm, $a = 126.8$, $b = 4000$.

3. Fabrication and measurement

The fabrication process is as follows. The SU-8 2002 is spin-coated on the PMMA substrate (the thermal softening temperature of the PMMA substrate is 115 °C) at a speed of 3000 r/min and pre baked at 65 °C for 10 min, and 90 °C for 20 min. Then the SU-8 is exposed to ultraviolet rays (ABM Co. Inc., USA) at a wavelength of 360 nm for 7 s and baked at 65 °C for 10 min and 90 °C for 20 min. The SU-8 is developed for 3 s in SU-8 developer and isopropanol. Then the waveguide is post-baked at 65 °C for 10 min and 90 °C for 20 min. The SEM photo of SU-8 waveguide core layer on PMMA substrate is shown in Fig. 6. The photo of the lithography mask of the AMZI waveguide is shown in Fig. 7.

The micro-reservoir layer is made on PMMA cladding chip (the thermal softening temperature of the PMMA cladding chip is 105 °C) by using CO_2 laser engraver (the cutting speed of the CO_2 laser engraver is 100 mm/s, the power is 25 W).[22] The micro reservoir is a rectangular groove structure on the PMMA chip. There are two holes on the micro reservoir. The micro-reservoir layer and the substrate layer are bonded by the nano-imprinting lithography (the bonding temperature at 110 °C, the imprinting pressure at 2 kg/cm^2, the imprinting time for 4 min). The packaging process has no effect on the surface structure of the SU-8 waveguide due to the high thermal softening temperature of SU-8. The end face of the bonded device is cut by the CO_2 laser engraver (the cutting speed of the CO_2 laser engraver is 15 mm/s, the power is 30 W). The fabrication and packaging process are shown in Fig. 8.

The schematic diagram and the photo of the AMZI rectangular waveguide sensor test system are shown in Fig. 9. The liquid flows from the input tube to the micro-reservoir, and flows through the output tube to the waste liquid bottle by the peristaltic pump (BT100-1L, Longer Precision Pump Co. Ltd., UK). Before and after the measurement, the deionized water is pumped into the micro-reservoir to clean it. The input optical signal is generated by the tunable laser (TSL-510, Santec, Co., JPN @1550 nm) and coupled into the sensor by the single mode fiber. The input optical power is 1 mW. The output signal of sensor is coupled into single mode fiber. The output optical fiber is connected to an optical power meter (AQ6317C, ANDO Co., Japan). Optical powermeter collects data and sends it to computer.

In order to verify the theoretical analysis of the output power in the range of 1.470–1.545, several different refractive index sucrose solutions are selected to test the sensor. Benzaldehyde ($n_1 = 1.545$) and ethanol ($n_2 = 1.362$) are mutually dissolvable in the mixture. These two kinds of liquids are mixed at different volume ratios to make mixtures with different refractive indices. The refractive index of each mixture is adjusted according to the following equation:

$$\frac{n^2-1}{n^2+2} = c_1 \cdot \frac{n_1^2-1}{n_1^2+2} + c_2 \cdot \frac{n_2^2-1}{n_2^2+2}, \tag{9}$$

where c_1 and c_2 are volume fractions, and n_1 and n_2 are refractive indices of benzaldehyde and ethanol. Relationships between the refractive index of each mixture and volume fractions are shown in Table 1.

Table 1. Relationship between the refractive index of analyte and volume fraction.

RIn	1.470	1.475	1.480	1.485	1.490	1.495	1.500	1.505
c_1	60.6%	63.4%	66.0%	68.7%	71.4%	74.1%	76.7%	79.3%
c_2	39.4%	36.6%	34.0%	31.3%	28.6%	25.9%	23.3%	20.7%
RIn	1.510	1.515	1.520	1.525	1.530	1.535	1.540	1.545
c_1	81.9%	84.5%	87.1%	89.7%	92.3%	94.9%	97.4%	100%
c_2	18.1%	15.5%	12.9%	10.3%	7.7%	5.1%	2.6%	0%

The insertion losses of the straight waveguide and MZ device fabricated via thermal bonding and laser polishing are 5.9 dB and 7.1 dB, respectively. And the simulation and experimental results are shown in Fig. 10. The insertion loss is between −80.36 dB and −10.63 dB. The variation tendencies of the simulation and experimental results are similar to each other, indicating that the fading region can be avoided by the proposed design. The length difference is optimized by the maximum output power difference between two interval endpoints in a range of 0 μm–20 μm, which means the

largest average slop of the curve. The slope of the linear region (1.495–1.545) is 548.95 dB/RIU and the average slope of the curve is 768.1 dB/RIU in the range of 1.470–1.545. The resolution of the optical power meter is 0.001 dB. The average and linear detection resolution are 1.30×10^{-6} RIU and 1.820×10^{-5} RIU, respectively.

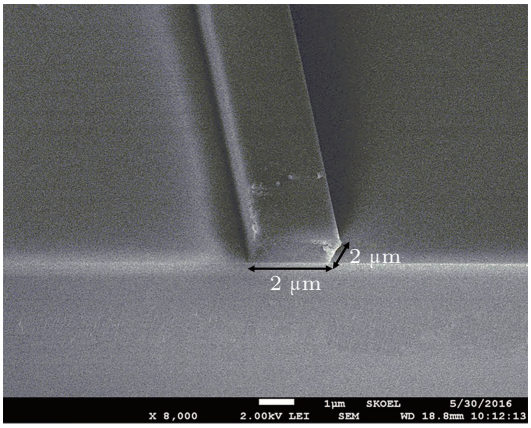


Fig. 6. SEM of SU-8 waveguide core layer with 2 μm×2 μm dimensions.

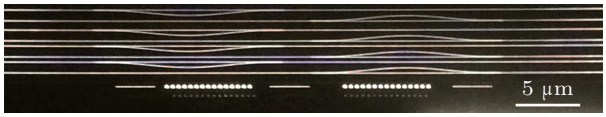


Fig. 7. Photo of the lithography mask of the AMZI waveguide.

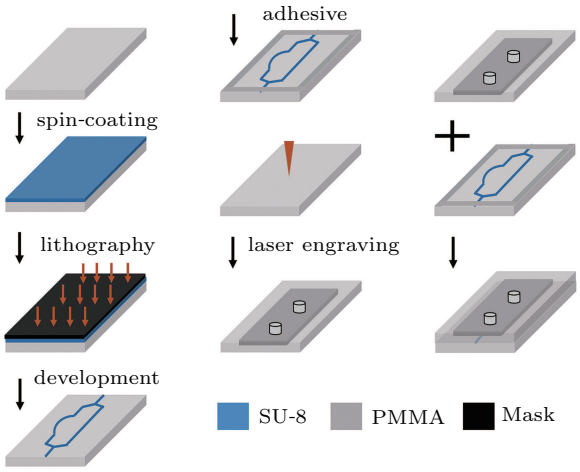


Fig. 8. (color online) Fabrication and packaging process of AMZI rectangular waveguide sensor.

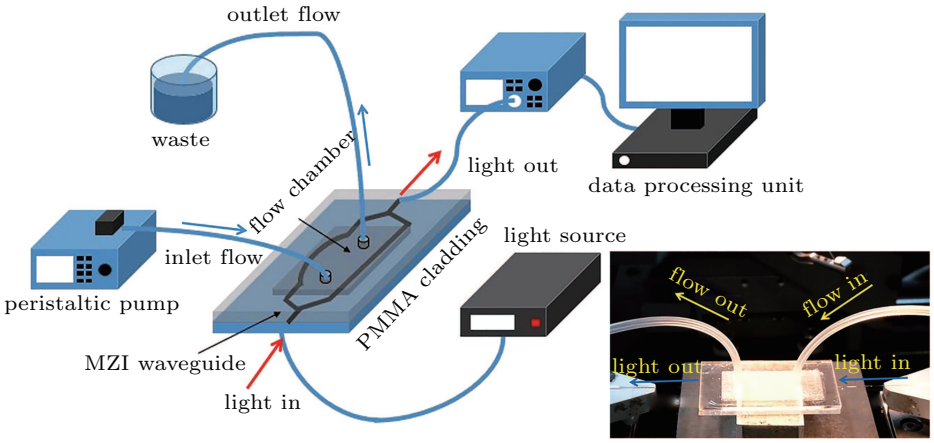


Fig. 9. (color online) Schematic diagram and photo of AMZI rectangular waveguide sensor test system.

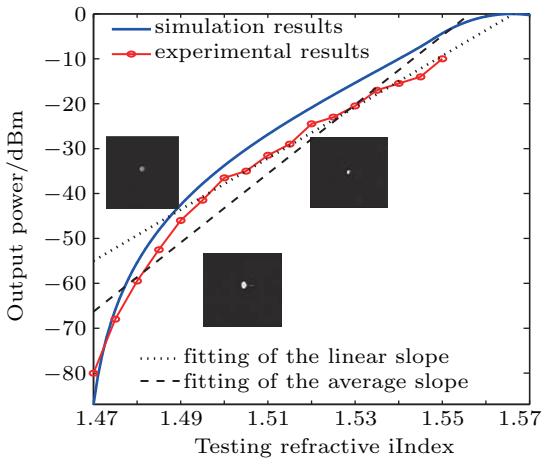


Fig. 10. (color online) Experimental and linear fit output power curve of the sensor with ΔL being 19.8 μm.

4. Conclusions and perspectives

In this paper, we present an all polymer AMZI waveguide sensor by the high efficiency and low cost imprinting bonding and laser polishing method. The waveguide of this sensor has three sensing surfaces contacting the test medium to increase the sensitivity. The length deviations between the sensing arm and the reference arm are optimized. When the length deviation is 19.8 μm, the average sensitivity is 768.1 dB/RIU in a sensing range of 1.470–1.545 and the average detection resolution is 1.3×10^{-6} RIU. This length deviation can reduce the size and transmission loss. Because of the fast and low fabrication process and the high sensitivity waveguide sensing structure, this waveguide sensor has advantages in the case requiring portability and disposability. In the following research, this sensor would be surface modified.

References

[1] Peter Kozma, Florian Kehl, Eva Ehrentreich–Förster, Christoph Stamm and Frank F Bier 2014 *Biosensors & Bioelectronics* **58** 287

[2] Jerome Hottin, Edy Wijaya, Laurent Hay, Sophie Maricot, Mohamed Bouazaoui and Jean-Pierre Vilcot 2013 *Plasmonics* **8** 619

[3] Srivastava T, Jha R and Das R 2011 *IEEE Photon. Technol. Lett.* **23** 1448

[4] Vala M, Chadt K and Piliarik M 2010 *Sensors & Actuators B: Chemical* **148** 544

[5] Huang Y H, Ho H P, Wu S Y, Kong S K, Wong W W and Shum P 2011 *Opt. Lett.* **36** 4092

[6] Wang R, Wang X X, Yang H and Ye S 2016 *Acta Phys. Sin.* **65** 094206 (in Chinese)

[7] Zhang X Q, Chen R S, Zhou Y, Ming H and Wang A T 2016 *Chin. Phys. Lett.* **33** 84201

[8] Wang J H, Chen C M, Zheng Y, Wang X B, Yi Y J, Sun X Q, Wang F and Zhang D M 2017 *Chin. Phys. B* **26** 024212

[9] Wales D J, Parker R M, Gates J C, Grossel M C and Smith P G R 2011 *The European Conference on Lasers and Electro-Optics*, May 22–26, 2011, Munich, Germany, p. 1

[10] Fan Y E, Zhu T, Shi L and Rao Y J 2011 *Appl. Opt.* **50** 4604

[11] Tiefenthaler K and Lukosz W 1989 *J. Opt. Soc. Am. B* **6** 209

[12] Jin L, Li M and He J J 2011 *Opt. Commun.* **284** 156

[13] Yang T, Wang T, Zheng C, Wang X and Zhang D 2014 *Microwave & Optical Technology Letters* **56** 1697

[14] Yang T F, Wang T J, Zheng C T, Wang X B and Zhang D M 2014 *Mod. Phys. Lett. B* **28** 1450044

[15] Shew B Y, Cheng Y C and Tsai Y H 2008 *Sensors & Actuators A Physical* **141** 299

[16] Bruck R, Melnik E, Muellner P, Hainberger R and Lämmerhofer M 2011 *Biosensors & Bioelectronics* **26** 3832

[17] Wang X B, Meng J, Sun X Q, Yang T F, Sun J, Chen C M, Zheng C T and Zhang D M 2012 *Appl. Surf. Sci.* **259** 105

[18] Ozhikandathil J and Packirisamy M 2014 *J. Electrochem. Soc.* **161** B3155

[19] Zhang J, Tan K L, Hong G D, Yang L J and Gong H Q 2001 *Journal of Micromechanics & Microengineering* **11** 20

[20] Zhao Y, Wang F, Cui Z C, Zheng J, Zhang H M, Zhang D M, Liu S Y and Yi M B 2004 *Microelectronics Journal* **35** 605

[21] Zheng H L and Chen F S 2005 *Semiconductor Optoelectronics* **26** 30

[22] Wang H R, Liu Y, Jiang M H, Chen C M, Wang X B, Wang F, Zhang D M and Yi Y J 2015 *Appl. Opt.* **54** 8412